Developmental Cell
Article

Death Receptors DR6 and TROY Regulate Brain Vascular Development

Stephen J. Tam,[1] David L. Richmond,[1] Joshua S. Kaminker,[2] Zora Modrusan,[3] Baby Martin-McNulty,[4] Tim C. Cao,[4] Robby M. Weimer,[4] Richard A.D. Carano,[4] Nick van Bruggen,[4] and Ryan J. Watts[1,*]
[1]Neurodegeneration Labs, Department of Neuroscience
[2]Bioinformatics
[3]Department of Molecular Biology
[4]Biomedical Imaging
Genentech, 1 DNA Way, South San Francisco, CA 94080, USA
*Correspondence: watts.ryan@gene.com
DOI 10.1016/j.devcel.2011.11.018

SUMMARY

Signaling events that regulate central nervous system (CNS) angiogenesis and blood-brain barrier (BBB) formation are only beginning to be elucidated. By evaluating the gene expression profile of mouse vasculature, we identified DR6/TNFRSF21 and TROY/TNFRSF19 as regulators of CNS-specific angiogenesis in both zebrafish and mice. Furthermore, these two death receptors interact both genetically and physically and are required for vascular endothelial growth factor (VEGF)-mediated JNK activation and subsequent human brain endothelial sprouting in vitro. Increasing beta-catenin levels in brain endothelium upregulate DR6 and TROY, indicating that these death receptors are downstream target genes of Wnt/beta-catenin signaling, which has been shown to be required for BBB development. These findings define a role for death receptors DR6 and TROY in CNS-specific vascular development.

INTRODUCTION

The vasculature of the CNS is an example of uniquely differentiated organ-specific blood vessels. CNS blood vessels differentiate to form the blood-brain barrier (BBB), which consists of a complex network of intercellular tight and adherens junctions that form a molecular seal between adjacent endothelial cells to limit molecular exchange across CNS vessels. Accordingly, the BBB has many transport mechanisms that enable specific jettisoning of unwanted molecules out of the CNS while importing molecules essential for brain function (Rubin and Staddon, 1999; Tam and Watts, 2010).

The molecular cues that regulate BBB development have remained elusive until recent findings described a role for the canonical Wnt/beta-catenin signaling cascade in CNS angiogenesis and barriergenesis (Daneman et al., 2009; Liebner et al., 2008; Stenman et al., 2008). These discoveries now raise a number of important questions related to BBB biology (Tam and Watts, 2010). For example, how does Wnt signaling regulate CNS angiogenesis and barriergenesis? Which molecules downstream of Wnt signaling drive BBB development? In addition to the canonical Wnt signaling components, these studies also identified tight junction proteins and transporters that may contribute to mature BBB function (Daneman et al., 2009, 2010).

We reasoned that gene expression profiling the BBB vasculature at embryonic, neonatal, and adult stages would enable identification of signaling molecules driving CNS vascular development. Subsquently, we show that death receptors DR6 and TROY are enriched in CNS vasculature during embryogenesis, and accordingly drive angiogenesis and barriergenesis in zebrafish and mouse model systems. Using an in vitro cell sprouting assay, we demonstrate that these two tumor necrosis factor (TNF) receptor family members are required for endothelial sprouting events in a cell-autonomous fashion through VEGF-mediated JNK activation of angiogenesis. Additionally, we find that DR6 and TROY genetically and physically interact, and may form a coreceptor complex at the BBB. Finally, we identify canonical Wnt/beta-catenin signaling as a key transcriptional regulator of DR6 and TROY BBB expression, suggesting one possible mechanism by which Wnt/beta-catenin transcription factor activity drives BBB angiogenesis and barriergenesis.

RESULTS

Identification of Genes Enriched in Brain Vasculature

To identify signaling molecules driving BBB development, maturation, and maintenance, we evaluated the gene expression profile of mouse vasculature at three distinct developmental time points (Figure 1A), corresponding to CNS angiogenesis (E14.5), astrocytic endfeet contact with cortical endothelium (P7.5), and maintenance of a mature BBB (Adult). We utilized florescence-activated cell sorting (FACS) to isolate CD31-positive, CD45-negative endothelial cells from mouse brain cortices, liver, and lung vasculature (Figure S1A available online), and subsequently verified FACS-mediated CNS vascular purification by qPCR analysis (Figure S1B). As expected, microarray analysis identified several Wnt/beta-catenin target genes and other previously characterized BBB-specific components to be enriched in BBB vasculature (Figure 1C; Figure S1) (Daneman et al., 2009; Hallmann et al., 1995; Pardridge et al., 1990).

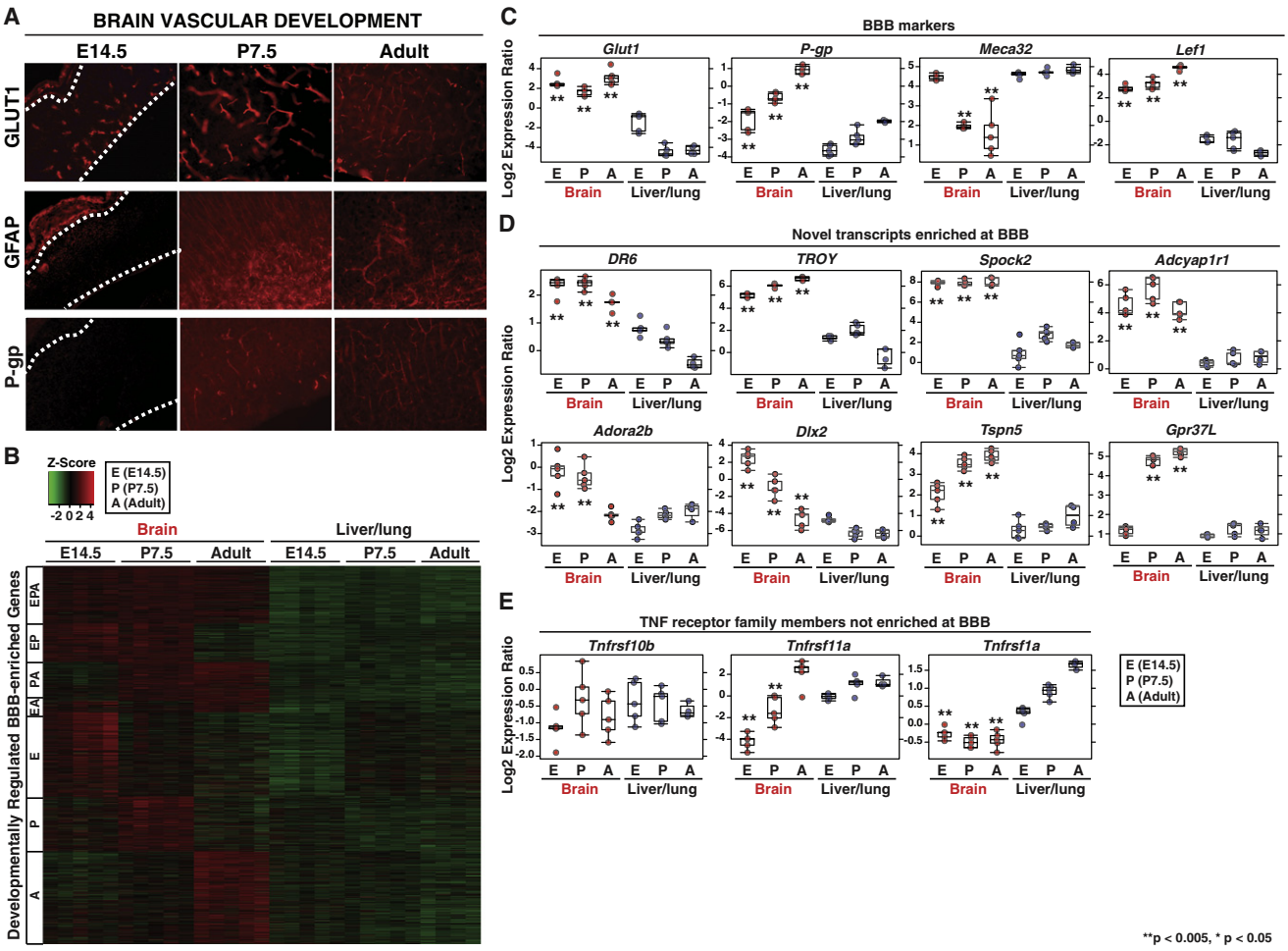

Figure 1. Blood-Brain Barrier Expression Profiling Identifies Genes Enriched in Brain Vasculature

(A) Three blood-brain barrier (BBB) developmental time points identified by immunohistochemical analysis of GLUT1 expression and astrocyte localization in the mouse cortex. (GLUT1, endothelial cells; GFAP, astrocytes; P-gp, P-glycoprotein) Results representative of at least three independent experiments are shown.

(B) Distinct developmentally regulated classes of BBB-specific transcripts were identified by microarray analysis. Samples are in columns; probes are in rows. Red and green color indicates over- or underexpression of probes in brain tissue relative to liver/lung tissue of the same stage, respectively. Developmental stage is indicated to the left of the heatmap (E, embryo; P, pup; A, adult). The probes shown in the heatmap are also presented in Table S1.

(C) Expression profiling FACS-purified BBB and liver/lung vasculature shows enrichment of BBB markers *Lef1*, *P-gp*, and *Glut1*.

(D) Selected transcripts enriched at the BBB.

(E) TNF receptor family members *Tnfrsf1a*, *10b*, and *11a* are not preferentially expressed in CNS vasculature. Box and whisker plots indicate distribution of data and highlight median (horizontal line through box) and the 25th and 75th quartiles (box edges). Expression values were compared between brain and liver/lung tissue at each developmental stage. Statistical significance was defined as those stage-specific comparisons yielding an adjusted p value (**$p < 0.005$; *$p < 0.05$). Further details of statistical analysis are described in extended Experimental Procedures. See also Figure S1 and Table S1.

Microarray analysis across the BBB developmental timeline was able to resolve gene expression changes in a spatiotemporal fashion (Figure 1B; Table S1; full microarray data set is publicly available at the NCBI Gene Expression Omnibus). For instance, while the CNS-specific glucose transporter *Glut1* is expressed in CNS at all three developmental time points, P-glycoprotein (*P-gp*) expression is highly upregulated at the BBB by postnatal day 7.5 (Figures 1A and 1C). Conversely, as *Meca32* is only expressed in fenestrated endothelium, transcript levels remained high in liver/lung vasculature at all time points and in embryonic brain vasculature, but are dramatically downregulated in brain vasculature by P7.5 and adult time points (Figure 1C) (Hallmann et al., 1995).

Further investigation of our gene expression data set yielded several classes of BBB-specific transcripts: upregulated exclusively at E14.5, P7.5, adulthood, p7.5 and adulthood (e.g., *Tspn5* and *Gpr37L*), E14.5 and P7.5 (e.g., *Adora2b* and *Dlx2*), and across all three developmental time points (e.g., *DR6*, *TROY*, *Spock2*, and *Adcyap1r1*) (Figures 1B and 1D; Table S1). Several of these transcripts have been previously described. For instance, both the proteoglycan SPOCK2 and homeobox transcription factor DLX2 have been shown to be expressed in CNS vessels and potentially drive CNS angiogenesis in a cell-autonomous fashion (Schnepp et al., 2005; Vasudevan et al., 2008). Notably, the death receptors *Tnfrsf21/DR6* and *Tnfrsf19/TROY* (Figure 1D; Figures S1D and S1E) were found to be highly

expressed in CNS-specific vasculature, while several TNF receptor family members including *Tnfrsf10b*, *Tnfrsf11a*, and *Tnfrsf1a* are not enriched in BBB vasculature (Figure 1E).

Zebrafish Candidate-Based Genetic Screen Identifies Regulators of CNS Angiogenesis and Barriergenesis

To understand the functional relevance of the BBB-specific transcripts identified in our expression profiling analysis, we employed a secondary screen utilizing the bony fish *danio rerio* (zebrafish) as a BBB developmental model system. Recently, zebrafish was shown to have a functional BBB as early as 3 days postfertilization (dpf), expressing ZO-1 and CLAUDIN-5 tight junction protein in CNS endothelia (Jeong et al., 2008). To directly visualize CNS vasculature we utilized *Kdrl-eGFP* transgenic zebrafish expressing green fluorescent protein in endothelial cells (Jin et al., 2005). We injected a solution containing 350 Da cationic DAPI and 10 kDa rhodamine-dextran into the common cardinal vein of 3 dpf zebrafish embryos and found dramatic retention of both dyes within CNS vasculature, whereas peripheral vessels exhibited gross leakage into the surrounding parenchymal space (Figures S2A and S2B) (Jeong et al., 2008). At this stage of development, blood vessels sprouting from the primordial hindbrain channels (PHBC) and basilar artery (BA) have formed an elaborate network of central arteries (CtA) in the brain (Figure 3C). Similar to the mammalian BBB, we found CNS-specific glucose transporter GLUT1 exclusively expressed in this vascular network (Figure 1; Figure S3F) (Pardridge et al., 1990).

Importantly, the zebrafish genome contains orthologs for murine BBB-enriched molecules *DR6*, *TROY*, *Spock2*, *Adcyap1r1*, and *Tspn5* (Figures S5A and S5B; data not shown), and mRNA transcripts and protein corresponding to *DR6* and *TROY* expression were detectable (Figures S3A, S3E, S5C, and S5D). Consistent with our murine expression profiling data, zebrafish DR6 was detected in CNS vasculature (Figures S3B and S3C). Therefore, we assessed CNS vasculature in 3 dpf embryos upon morpholino-mediated knockdown of these BBB-specific molecules at the developing zebrafish BBB (Figures S3A and S5C). Protein translation was sterically inhibited through translation-blocking antisense hybridization with mRNA start codon. Loss of function of BBB-enriched *DR6*, *TROY*, *Spock2*, *Adcyap1r1*, and *Tspn5* all resulted in robust CNS-specific defects in vessel arborization, whereas trunk intersegmental vessels (ISVs) were unperturbed (Figures 2A and 2B). Conversely, *Tnfrsf1a* (a TNF receptor family member that was not enriched at the BBB) knockdown embryos were indistinguishable from control embryos.

During vascular sprouting into the developing CNS many features specific to BBB function are initiated (Virgintino et al., 2007). At the earliest stages of CNS angiogenesis, BBB components such as CLAUDIN-5 and GLUT1 are present along with a physical barrier that can exclude small molecules from entering the embryonic CNS (Daneman et al., 2009; Ek et al., 2006). Therefore, our findings that DR6, TROY, SPOCK2, ADCYAP1R1, and TSPN5 modulate CNS vascular development suggested that these BBB-specific components may also regulate CNS barriergenesis. To test this possibility, microangiographic injections of leakage tracers DAPI and rhodamine-dextran were performed on 3 dpf knockdown zebrafish embryos followed by confocal live imaging of the CNS. Whereas control, *Adcyap1r1*, *Tspn5*, and *Tnfrsf1a* morphant embryos excluded most of these tracers, as rhodamine-dextran was restricted to CtA vessel lumen while DAPI-stained nuclei were only found in CtA vessels, *DR6*, *TROY*, and *Spock2* morphants exhibited dramatic leakage of both tracers across the BBB, as evidenced by an increase in rhodamine-dextran signal and parenchymal nuclear staining by DAPI (Figure 2A). Quantification of BBB leakage was accomplished by counting the number of DAPI-positive parenchymal nuclei in the zebrafish brain. We observed a greater than 5-fold increase in DAPI leakage across the BBB upon *DR6*, *TROY* and *Spock2* knockdown compared to control embryos (Figure 2C). These findings support a role for DR6, TROY, and SPOCK2 in CNS vascular development.

DR6 Is Necessary for CNS Angiogenesis in Zebrafish

We next set out to quantify zebrafish brain and trunk vasculature in response to DR6 loss of function. Consistent with the results from our screen, 2D quantification of 3 dpf zebrafish CNS and trunk vasculature revealed that the number of hindbrain CtAs per brain, but not trunk ISV density, was reduced upon DR6 knockdown (Figures 3A and 3B). Likewise, fractional vessel heights were only reduced in the CNS.

As vascular arborization is a product of coordinated sprouting, branching, and lumenization (Adams and Alitalo, 2007), we asked which of these processes are driven by DR6 by reconstructing 3D confocal z stacks imaged from the developing zebrafish CNS vasculature and computationally measured the CtA density, branch density, and vessel diameter in response to DR6-targeting morpholinos (Figure 3C). While both CtA vessel diameter and branch density were not significantly altered upon *DR6* knockdown, vascular density was decreased approximately 30% compared to control morpholino-injected embryos (Figures 3D). Furthermore, time-lapse imaging of 1.5–3 dpf embryos suggests that DR6 is required for initial CtA sprouting events from the BA and PHBC vascular networks, but not required to inhibit vascular regression or degeneration (Movies S1, S2, S3, and S4). While *DR6* knockdown phenotypes could not be rescued upon *DR6* overexpression, as death receptors are acutely cytotoxic at high levels (Lavrik et al., 2007; Pan et al., 1998), the specificity of *DR6* knockdown phenotypes was verified using another nonoverlapping translation blocking morpholino, as well as a splice-blocking morpholino that leads to efficient pre-mRNA exon deletion in *DR6* transcripts and similar defects in CNS angiogenesis and barriergenesis (Figures S3D, S3E, S4E, and S4F). We conclude that DR6 is required for CNS-specific angiogenesis, primarily through regulation of sprouting activity, but not through regression, anastamosis, or lumenization.

DR6 Is Required for Proper CNS Vascular Density and Barrier Function in Mice

We next examined DR6 expression in the developing mouse CNS vasculature. Immunohistochemistry (Figure 4A; Figure S4A), *DR6.eGFP* knockin expression (Figure S5F) and in situ hybridization (Figure 4B) confirmed that DR6 is not only expressed in neurons, particularly commissural axons in the developing spinal cord, but also in CNS-specific vasculature (double labeling with GLUT1), suggesting that DR6 might be

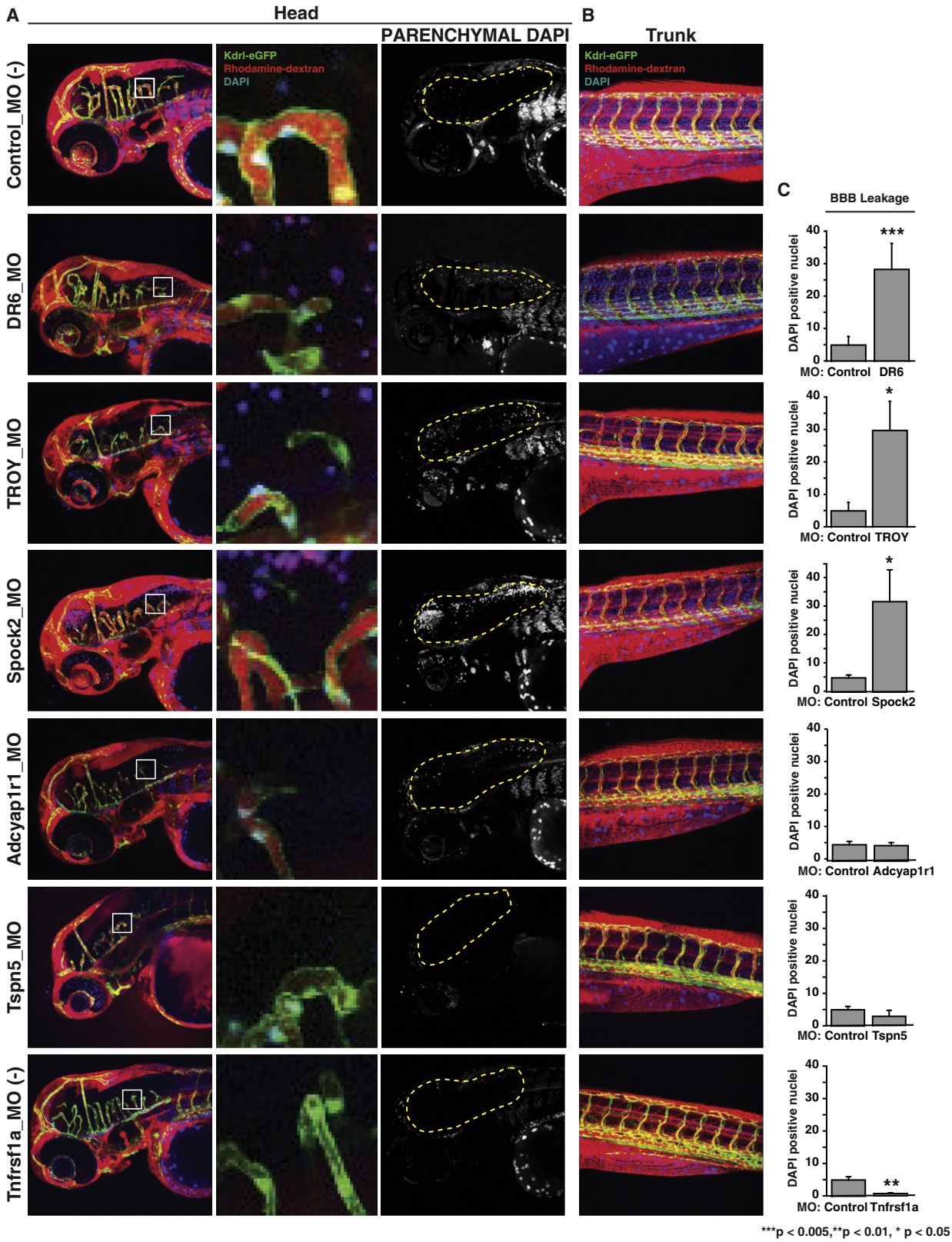

Figure 2. Zebrafish Candidate-Based Genetic Screen Identifies Regulators of CNS Angiogenesis and Barriergenesis

(A and B) Morpholino-mediated knockdown of BBB-enriched transcripts in *Tg(kdrl:egfp)* embryos. As described in Experimental Procedures, following a 4 ng morpholino injection, DAPI-positive brain parenchymal nuclei (Parenchymal DAPI; A: right panels) were visually isolated by computationally removing brain

necessary for murine CNS vascular patterning and/or barrier function.

In order to elucidate the functional relevance of DR6 enrichment in mouse BBB vasculature, we characterized both vascular density and barrier function in *DR6* knockout mice. Ex vivo X-ray microcomputed tomography (micro-CT) angiography was used to quantitatively measure the whole-brain 3D cerebral vascular structure. Importantly, we found that adult *DR6* knockout mice exhibit ~30% decrease in brain vascular density compared to wild-type littermates (Figures 4C and 4D; Figure S4B). This defect is similar to vascular density reduction in zebrafish embryos upon *DR6* knockdown (Figure 3D; Figure S3D).

Our findings that DR6 is required for proper CNS vascular density in the mature mouse brain, and drives both CNS angiogenesis and barriergenesis during zebrafish development suggest that DR6 may also regulate CNS barrier function in the adult mouse. To test this possibility, we evaluated whether *DR6* knockout mice also have a disrupted BBB by quantifying CNS extravasation of intravenously injected Evans blue dye, as previously described (Eliceiri et al., 1999). Even though *DR6* KO adult mice are viable, these animals exhibited an approximately 2-fold increase in Evans blue dye leakage compared to wild-type littermate controls (Figure 4E), which is similar in magnitude to barrier deficits observed after intracortical delivery of VEGF (Figure S4C), a well-known cytokine that induces vascular permeability. Therefore, we conclude that DR6 contributes to CNS vascular morphogenesis and barrier function in mice.

To determine if DR6 loss-of-function phenotypes in adult mice may be a consequence of dysregulated CNS angiogenesis and barriergenesis during development, we investigated possible embryonic phenotypes. Indeed, *DR6* knockout embryos exhibited both forebrain-specific hemorrhaging events (Figure 4F) as well as an ~15% increase in sulfo-NHS-biotin leakage across the BBB upon transcardiac perfusion (Figure 4G). Furthermore, embryonic hindbrain radial vessel density was significantly reduced in *DR6* knockout embryos (Figures 4H and 4I). To determine if these phenotypes arise as a consequence of DR6 specifically in endothelial cells, we generated a floxed exon2 *DR6* allele and crossed it to a *Tie2-Cre* mouse driver line to remove DR6 from endothelium in vivo. Similar to our observations in *DR6* knockout embryos (Figures 4F, 4H, and 4I), we find that endothelial-specific *DR6* deletion in $DR6^{flox/flox}$;*Tie2-Cre* embryos recapitulated the *DR6* null phenotype with forebrain-specific hemorrhaging events at E11.5 and reduced hindbrain radial vessel density (Figures 4J–4L). Furthermore, we observed that both the *DR6* knockout and the endothelial-specific *DR6* conditional knockout show a reduction in tight junction component ZO-1 protein levels (Figure S7B). These early developmental BBB phenotypes are consistent with the idea that DR6 is an essential regulator of BBB development in a cell-autonomous fashion.

Intriguingly, amyloid precursor protein (APP), a candidate DR6 ligand that was proposed to drive developmental axon degeneration in neurons (Nikolaev et al., 2009), was identified in our expression profiling data to be modestly enriched in BBB vasculature exclusively during embryogenesis, and somewhat downregulated in adult CNS vasculature, relative to liver/lung vascular expression (Figure S4D). To determine whether APP drives DR6 activity during BBB development, we asked if *APP* and *DR6* deletions share similar BBB developmental phenotypes. We found that while *APP* loss of function in zebrafish and mice exhibited subtle vascular abnormalities (Figures S4E, S4G, and S4H), *APP* loss of function did not result in BBB leakage (Figures S4E–S4G). We conclude that APP is not required for CNS barriergenesis and therefore likely does not drive DR6 activity during BBB development.

Cell-Autonomous Regulation of Vascular Sprouting by DR6

In order to examine the contribution of endothelial cell-derived DR6 toward BBB development in more detail, we utilized an in vitro human brain microvascular endothelial cell (HBMEC) sprouting assay that we established whereby primary HBMECs were coated onto cytodex beads and allowed to sprout in a 3D fibrin matrix. In a similar fashion to DR6, Neuropilin-1 (NRP1) has been demonstrated to guide the development of both the nervous and vascular systems (Gu et al., 2003; Tam and Watts, 2010). Accordingly, function-blocking antibodies targeting NRP1 strongly inhibited HBMEC vascular remodeling and sprouting, which confirmed HBMEC sprouting activity to be NRP1-dependent (Figure 5A) (Pan et al., 2007). Importantly, two distinct function-blocking antibodies targeting DR6 directly inhibited the number of sprouting HBMECs and their mean sprout length to a similar extent as anti-NRP1 antibody treatment (Figure 6A; Figure S6C). Furthermore, siRNA-mediated knockdown of *DR6* yielding >70% reduction in transcript and protein levels (Figures S6A and S6B), also significantly reduced HBMEC sprout length and cell number (Figure 5B), albeit to a lesser extent than anti-DR6 function-blocking antibodies. These results suggest that during BBB development, DR6 directs brain vascular development and barriergenesis through regulation of sprouting in a cell-autonomous fashion.

TROY Is Necessary for CNS Angiogenesis

Based on our DR6 results and data from our zebrafish screen, we speculated that another death receptor, TROY, may work in concert with DR6 to regulate CNS vascular development. Consistent with our zebrafish screening results (Figure 2), 2D quantification of 3 dpf zebrafish CNS and trunk vasculature revealed that the number of hindbrain CtAs per brain, but not trunk ISV density, was reduced upon *TROY* knockdown (Figures 5C and 5D). Likewise, fractional vessel heights were only reduced in the CNS. While brain vascular density decreased by ~30% in response to *TROY*-targeting morpholino, there were no significant defects with respect to CtA branch density or vessel diameter (Figure 5E). Time-lapse imaging of 1.5–3 dpf embryos also

vasculature-derived DAPI signal from the DAPI channel. Results representative of at least three independent experiments are shown. Endothelial cells are green, DAPI is blue, rhodamine-dextran is red. MO, morpholino.

(C) Quantification of DAPI leakage across the zebrafish BBB. n = 6 (control_MO), n > 6 (DR6_MO, TROY_MO, Spock2_MO, Adcyap1r1_MO, Tspn5_MO, and Tnfrsf1a_MO).

Data are presented as the mean ± standard error of the mean (SEM) (***$p < 0.005$; **$p < 0.01$; *$p < 0.05$). See also Figure S2.

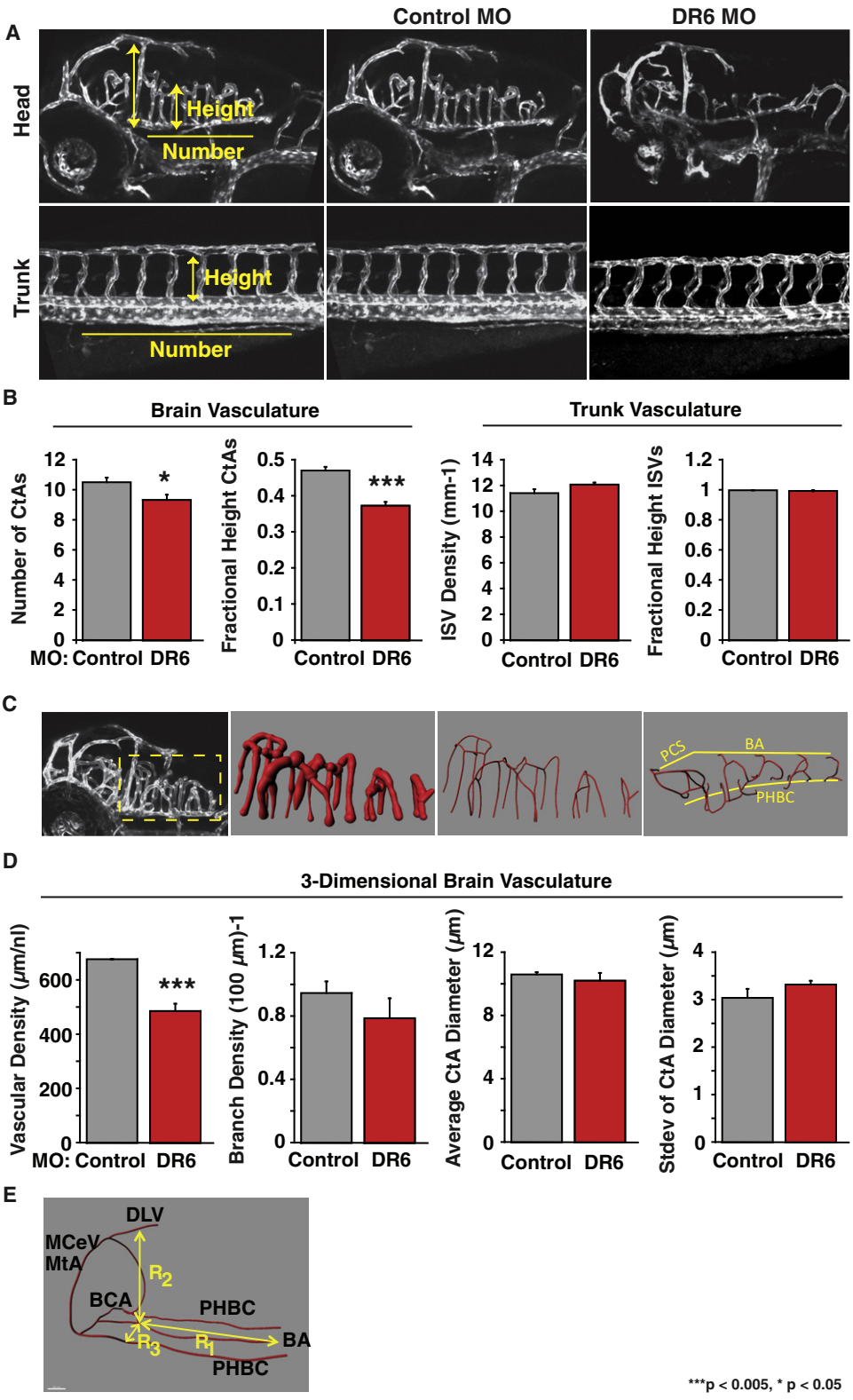

Figure 3. Zebrafish Blood-Brain Barrier Requires DR6 for CNS Angiogenesis

(A) Translation-blocking morpholino-mediated DR6 knockdown leads to CNS-specific angiogenic defects in *Tg(kdrl:egfp)* embryos. Each embryo was treated with 4 ng morpholino. Results representative of at least three independent experiments are shown. MO, morpholino; CtA, central artery; ISV, intersegmental vessels. (B) 2D quantification of 3 dpf zebrafish CNS and trunk vasculature. n = 36 (control_MO), n = 15 (DR6_MO), see Experimental Procedures, Zebrafish Microangiographic Imaging and Quantification, for calculation of the fractional height of CtAs and ISVs.

suggested that TROY is required for initial CtA sprouting events but not for degenerative developmental processes during CNS vessel formation (Movies S5 and S6). We verified morpholino-mediated knockdown using a splice-blocking morpholino, which inhibits splicing events in *TROY* transcripts and resulted in similar defects in CNS angiogenesis and barriergenesis (Figure S5D).

To further establish that TROY plays a role in CNS vascular biology we evaluated both *TROY* knockout mice phenotypes and TROY regulation of angiogeneic sprouting in the HBMEC bead assay. Adult *TROY* knockout mice exhibited a modest increase in Evans blue dye BBB leakage compared to wild-type littermate controls (Figure 5F). Furthermore, siRNA-mediated knockdown of *TROY* yielding >85% reduction in transcript levels (Figure S6A) significantly reduced HBMEC sprout length and cell number (Figure 5B). Therefore, similar to DR6, TROY is required for CNS-specific angiogenesis, primarily through regulation of sprouting activity, but not through regression, anastamosis, or lumenization.

DR6 and TROY Physically Interact

As DR6 and TROY loss of function shared similar CNS vasculature developmental defects in zebrafish and sprouting defects in vitro, we hypothesized that DR6 and TROY may form functional coreceptors. Specific TNF receptors have been shown to heteromultimerize with other family members, as well as other signaling receptor families. For instance, TNF receptor family member p75 inhibits axon regeneration through Nogo-66 receptor (NgR1) binding (Wang et al., 2002). TNF receptor TROY can also form a receptor complex with NgR1 and functionally replace p75 in neurons (Park et al., 2005; Shao et al., 2005). Indeed, when transfected into COS7 cells, TROY can be coimmunoprecipitated with NgR1 (Figure 6A). Notably, TROY appeared to homo-oligomerize upon transfection as HA-tagged TROY could pulldown flag-tagged TROY. Consistent with our prediction, transfected DR6 strongly coimmunoprecipitated with TROY to an even greater degree than compared to positive control NgR1 (Figure 6A). Furthermore, both anti-DR6 function-blocking antibodies that were used to inhibit HBMEC sprouting were able to partially block DR6/TROY binding (Figure 6B). Considering that purified DR6 extracellular domains did not directly bind to TROY-expressing 293 cells (Figure S6D), we propose a model whereby DR6 and TROY physically interact through their cytoplasmic or transmembrane domains to form a functional receptor complex in CNS vascular development.

DR6 and TROY Genetically Interact

Having shown that DR6 and TROY physically interact, we next examined their potential genetic interactions. We coinjected *DR6* and *TROY* targeting morpholinos at suboptimal concentrations that individually caused no detectable defects in zebrafish CNS vessel formation and barrier function (Figures 6C and 6D). Embryos coinjected with both morpholinos at these concentrations displayed synergistic CNS-specific vascular defects and barrier leakage. In other words, simultaneous suboptimal *DR6* and *TROY* knockdown unmasked otherwise silent BBB-specific phenotypes that resulted in an enhanced genetic interaction similar to yeast gene function mapping studies identifying gene deletion pairs that uncover sick/lethal synthetic phenotypes (Tong et al., 2001). The identification of both BBB-specific genetic and physical interactions between DR6 and TROY suggests that binding partners DR6 and TROY function in unison to contribute to CNS angiogenesis and barriergenesis during development.

DR6 and TROY Are Required for VEGF-Mediated JNK Activation and Subsequent Human Brain Endothelial Sprouting

Mediated largely through proangiogenic factor VEGF binding to cognate receptor VEGFR2, sprouting angiogenesis requires the orchestration of a number of cellular events that are integrated by molecular signals including cellular migration via p38 (Rousseau et al., 1997), proliferation via ERK (Rousseau et al., 1997; Takahashi et al., 1999), and survival/vascular permeability via PI3-kinase/AKT (Chen et al., 2005; Gerber et al., 1998; Six et al., 2002). Interestingly, wild-type or dominant-negative ERK2 overexpression triggers enhancement or suppression of JNK activation, respectively, which demonstrates that VEGF-mediated ERK phosphorylation activates downstream JNK (Pedram et al., 1998). Accordingly, JNK activation has since been identified as a positive regulator of human umbilical vein endothelial cell (HUVEC) angiogenesis (Uchida et al., 2008; Wu et al., 2006). Indeed, we found that VEGF strongly stimulates JNK activation in HBMECs, as evidenced by increased phospho-JNK levels (Figure 6E). In order to verify the hypothesis that JNK activation is required for efficient brain vessel sprouting, two structurally distinct and highly selective JNK inhibitors (JNK-V and JNK-VIII) were individually tested in the HBMEC bead-sprouting assay (Gaillard et al., 2005; Szczepankiewicz et al., 2006). Upon addition of each JNK inhibitor, we found robust inhibition of both HBMEC sprout length and sprouting cell number to a similar degree as *DR6* and *TROY* knockdown (Figure 6F).

While death receptors are typically thought to functionally interact with the cellular apoptosis machinery, different cellular environments can shift death receptors toward mediating functions distinct from, or even against cell death (Ashkenazi and Dixit, 1998). For instance, TNF binding to death receptor TNFR1 activates NF-κB signaling which in turn suppresses TNF-induced apoptosis (Beg and Baltimore, 1996). Only upon sufficient suppression of NF-κB signaling can TNF-TNFR1 induce cell death. Additionally, death receptor TNFRSF6/CD95 has recently been shown to promote tumor cell proliferation

(C) 3D reconstructions of zebrafish hindbrain vasculature were used to create a vascular mask (second panel from the left) to determine vascular density and average CtA diameter. Filament tracing of the vessel-derived eGFP signal (first and second panels from the right) enabled branch density calculations.
(D) 3D quantification of 3 dpf zebrafish hindbrain vasculature. Standard deviation of CtA diameter is a metric of irregularity in vessel lumenization. n = 4 (control_MO), n = 6 (DR6_MO).
(E) Zebrafish brain volume calculation diagram. The volume of the half brain was approximated as $V = R_1R_2R_3$. MtA, metencephalic artery; MCeV, middle cerebral vein; DLV, dorsal longitudinal vein; BCA, basal communicating artery; PHBC, primordial hindbrain channel; BA, basilar artery.
Data are presented as the mean ± SEM (***p < 0.005; *p < 0.05). See also Figure S3 and Movies S1, S2, S3, and S4.

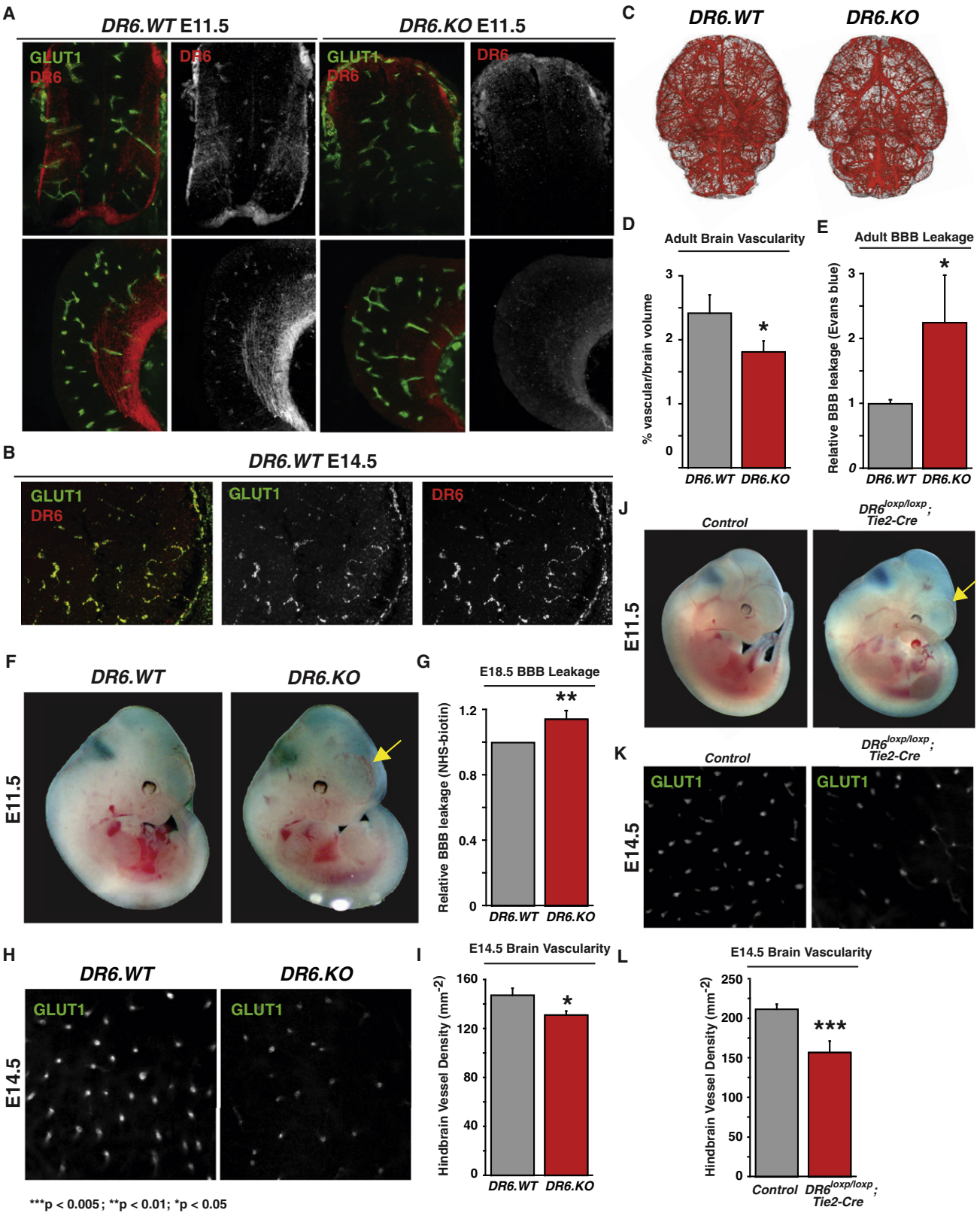

Figure 4. DR6 Is Required for Proper CNS Vascular Density and Barrier Function in Mice in a Cell-Autonomous Fashion

(A) DR6 protein expression in CNS commissural axons and GLUT1-positive vasculature. Immunohistochemical staining for DR6 protein exhibited both neuronal and vascular signal in spinal cord (top panels) and forebrain (bottom panels) tissue from E11.5 embryos. This signal is specific to DR6 protein, as no antibody

through downstream JNK activation (Chen et al., 2010). The dual functions of CD95 can be explained by the observation that CD95-mediated apoptosis requires 1,000-fold higher protein levels compared to its nonapoptotic activity (Lavrik et al., 2007). Therefore, the cellular consequences of death receptor activation of downstream signaling pathways function in a context-dependent manner. The death receptors DR6 and TROY were initially identified as JNK-activating members of the TNFR superfamily that promote cell death (Eby et al., 2000; Pan et al., 1998). Interestingly, JNK2/3 double knockouts have been previously described to exhibit gross vascular defects (Laukeviciene et al., 2006). Therefore, we reasoned that DR6 and TROY might promote CNS angiogenesis through nonapoptotic JNK activation.

In order to delineate potential signaling crosstalk between VEGF-VEGFR2 and these BBB-specific death receptors, proangiogenic signaling pathways were examined in HBMECs transfected with siRNA against either *DR6* or *TROY* followed by VEGF addition. VEGF-mediated activation of ERK, AKT, or p38 signaling was not modified upon *DR6* or *TROY* knockdown (Figure 6E). However, consistent with previous cell culture studies demonstrating JNK activation upon DR6 or TROY overexpression (Eby et al., 2000; Pan et al., 1998), we found that VEGF-mediated JNK phosphorylation was reduced upon abrogation of *DR6* or *TROY* expression in human brain endothelial cells (Figure 6E, right). These results are consistent with the finding that DR6 and TROY are required for VEGF-mediated JNK activation and subsequent human brain endothelial sprouting.

DR6 and TROY Are Downstream of Canonical Wnt/Beta-Catenin Signaling in CNS Vasculature

Recently, canonical Wnt/beta-catenin signaling was identified as a key regulator essential for CNS-specific angiogenesis, barriergenesis, and GLUT1 expression at the BBB in a cell-autonomous fashion (Daneman et al., 2009; Liebner et al., 2008; Stenman et al., 2008). Intriguingly, we found that *DR6* and *TROY* knockouts maintain high levels of GLUT1 expression, low levels of vesicular-protein PLVAP, normal PDGFRbeta-positive pericyte and tight junction protein localization within CNS vasculature (Figure 4A; Figures S3F, S5E, and S7), suggesting that the Wnt/beta-catenin pathway is likely not downstream of DR6 and TROY signaling. However, we found that *DR6* and *TROY* knockouts exhibit reduced ZO-1 protein levels, which suggests that these death receptors may regulate brain vascular development partially through tight-junction component modulation (Figure S7B).

We next investigated whether the Wnt signaling pathway drives CNS angiogenesis and barrier formation in part by modulating *DR6* and *TROY* expression at the BBB. To examine the possibility that these two death receptors are downstream effectors that partially account for Wnt/beta-catenin involvement in BBB development, we measured *DR6* and *TROY* transcript levels in response to recombinant hWnt3a ligand, hWnt3a conditioned media, and GSK3beta inhibitor SB216763 in HBMECs. In a similar fashion to canonical Wnt target gene *Axin2*, *DR6* and *TROY* were significantly upregulated in response to two different forms of exogenous Wnt3a ligand, as well as pharmacological stabilization of beta-catenin by SB216763 (Figures 7A, 7B, and 7D). Furthermore, Wnt3a-mediated transcriptional upregulation of these two BBB-specific death receptors was completely reversible upon siRNA-mediated *beta-catenin* knockdown or addition of the pan-Wnt ligand binding soluble Fzd8-Fc protein (Figures 7C and 7D) (DeAlmeida et al., 2007; Gong et al., 2010).

The Wnt/beta-catenin developmental pathway employs expression feedback loops to enable temporal autoregulation through Wnt-responsive gene expression (Logan and Nusse, 2004). In light of our findings that *DR6* and *TROY* are Wnt-responsive genes, we reasoned that DR6 and TROY may also participate in Wnt signaling autoregulation. A prediction of this idea is that death receptor loss of function would modulate brain vascular Wnt target gene expression levels. Indeed, expression analysis of FACS-purified brain vasculature revealed that *DR6* knockout BBB vasculature exhibit marked reduction of two canonical Wnt target gene transcripts, *Apcdd1* and *Axin2* (Figure 7E). However, given that Wnt-driven GLUT1 expression is largely unaffected upon DR6 or TROY loss of function (Figure 4A;

staining was apparent in *DR6.KO* embryos (right panels). Results representative of at least three independent experiments are shown. WT, wild-type; KO, knockout.

(B) *DR6* mRNA expression in *Glut1*-positive vasculature. Dual-target two-color fluorescent in situ hybridization was used to detect *DR6* (red) and *Glut1* (green) transcripts in mouse E14.5 brains. Results representative of at least three independent experiments are shown.

(C) MicroCT angiographic surface renderings of adult mouse brain vasculature. 2D projections of *DR6.WT* and *DR6.KO* brains are shown. Results representative of six independent experiments are shown.

(D) Quantification of microCT CNS vascular network. Vascular density was calculated as a function of vascular volume normalized by brain volume. n = 6 (*DR6.WT*), n = 6 (*DR6.KO*).

(E) Evans blue leakage assay detects barrier defects in adult mice. n = 7 (*DR6.WT*), n = 8 (*DR6.KO*).

(F) E11.5 *DR6.KO* embryos exhibit forebrain-specific hemorrhaging (observed in 60% embryos tested; arrow). Results representative of at least three independent experiments are shown.

(G) Fixable biotin transcardiac perfusion assay detects barrier defects in E18.5 mouse embryos. n = 12 (*DR6.WT*), n = 12 (*DR6.KO*).

(H) *DR6.KO* embryos exhibit reduced hindbrain vascular density at E14.5. Confocal images of flat-mounted hindbrains representative of at least nine independent experiments are shown.

(I) Quantification of E14.5 mouse hindbrain vascular density. Vascular density was calculated as a function of number of GLUT1-positive hindbrain radial vessels normalized by field area. n = 12 (*DR6.WT*), n = 11 (*DR6.KO*).

(J) E11.5 $DR6^{flox/flox}$;*Tie2-Cre* embryos exhibit forebrain-specific hemorrhaging (observed in 80% embryos tested; arrow). Results representative of at least three independent experiments are shown.

(K) E11.5 $DR6^{flox/flox}$;*Tie2-Cre* embryos exhibit reduced hindbrain vascular density at E14.5. Confocal images of flat-mounted hindbrains representative of at least nine independent experiments are shown.

(L) Quantification of E14.5 mouse hindbrain vascular density. Vascular density was calculated as described above. n = 15 (control), n = 11 ($DR6^{flox/flox}$;*Tie2-Cre*). Data are presented as the mean ± SEM (***$p < 0.005$; **$p < 0.01$; *$p < 0.05$). See also Figure S4.

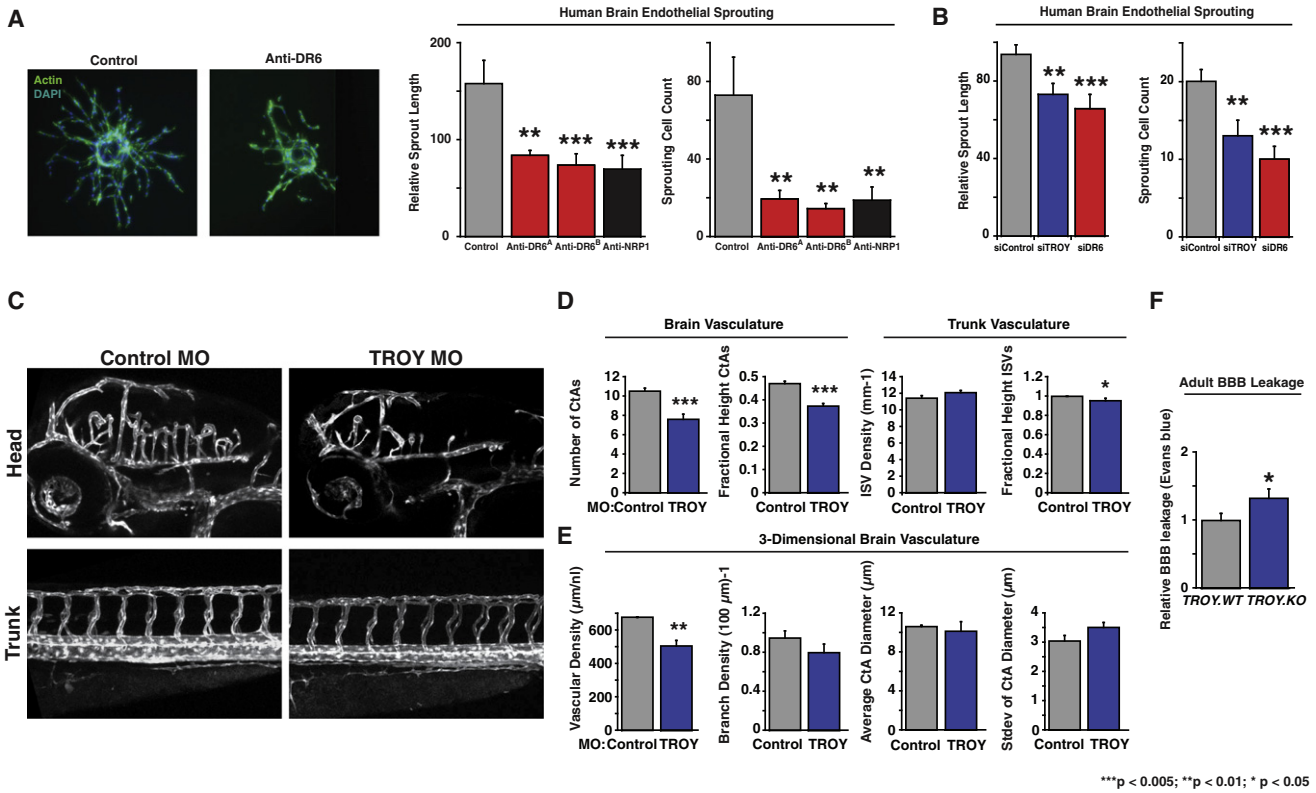

Figure 5. DR6 and TROY Are Required for Proper CNS Vascular Density and Barrier Function through Brain Endothelial Angiogenic Sprouting in a Cell-Autonomous Fashion

(A) Anti-DR6 function-blocking antibodies reduce HBMEC sprouting. Actin is green, nuclei are blue (left). Results representative of at least three independent experiments are shown. Quantification of sprout length (middle) and number of sprouting cells (right) are shown.

(B) siRNA-mediated knockdown of *DR6* and *TROY* inhibits HBMEC sprouting.

(C) Translation-blocking morpholino-mediated *TROY* knockdown leads to CNS-specific angiogenic defects. Each *Tg(kdrl:egfp)* zebrafish embryo was treated with 4 ng morpholino. Results representative of at least three independent experiments are shown.

(D) 2D quantification of 3 dpf zebrafish vasculature. n = 36 (control_MO), n = 25 (TROY_MO).

(E) 3D quantification of 3 dpf zebrafish hindbrain vasculature. n = 5 (control_MO), n = 6 (TROY_MO).

(F) Evans blue leakage assay detects barrier defects in adult mice. n = 16 (TROY.WT), n = 18 (TROY.KO).

Data are presented as the mean ± SEM (***p < 0.005; **p < 0.01; *p < 0.05). See also Figure S5 and Movies S5 and S6.

Figures S3F and S5E), DR6-mediated autoregulation of Wnt signaling at the BBB may only have modest functional relevance and therefore requires more detailed investigation. In conclusion, we find that *DR6* and *TROY* expression is regulated by canonical Wnt/beta-catenin signaling at the BBB, thereby driving BBB-specific activity of these death receptors to contribute toward CNS angiogenesis and barriergenesis during development (Figure 7F).

DISCUSSION

A Progrowth/Morphogenic Role for Death Receptors

The death receptor CD95 has been shown to function in direct opposition to, or even entirely independent of necrotic cell death (Chen et al., 2010). Similarly, we find that DR6 and TROY promote BBB development, independent of their canonical pro-degenerative or apoptotic activities. We therefore propose that nonapoptotic activity mediated by death receptors may be a general property inherent to these signaling molecules. Specifically, death receptors may act as cell fate switches that amplify signaling toward either proliferation or caspase-mediated cell death through context-dependent molecular cues. Alternatively, the cellular functions of these receptors may be predetermined within specific cell types. For instance, DR6 and TROY might not be able to engage the apoptotic machinery in endothelial cells.

Although Wnt/beta-catenin signaling is indispensible for BBB-specific GLUT1 expression, we find that DR6 and TROY are not. How then do DR6 and TROY contribute to CNS vessel and barrier formation at the molecular level? Are the barrier defects associated with DR6 and TROY loss of function a direct consequence of vascular developmental defects, or do these death receptors drive CNS angiogenesis and barriergenesis independently? Although *DR6*, *TROY*, and *Spock2* knockdown resulted in both vascular and barrier defects, BBB-enriched molecules *Adcyap1r1* and *Tspn5* knockdown exhibited gross brain vascular malformations in the absence of barrier leakage phenotypes, suggesting that impaired CNS vascular development does not inevitably inhibit BBB formation.

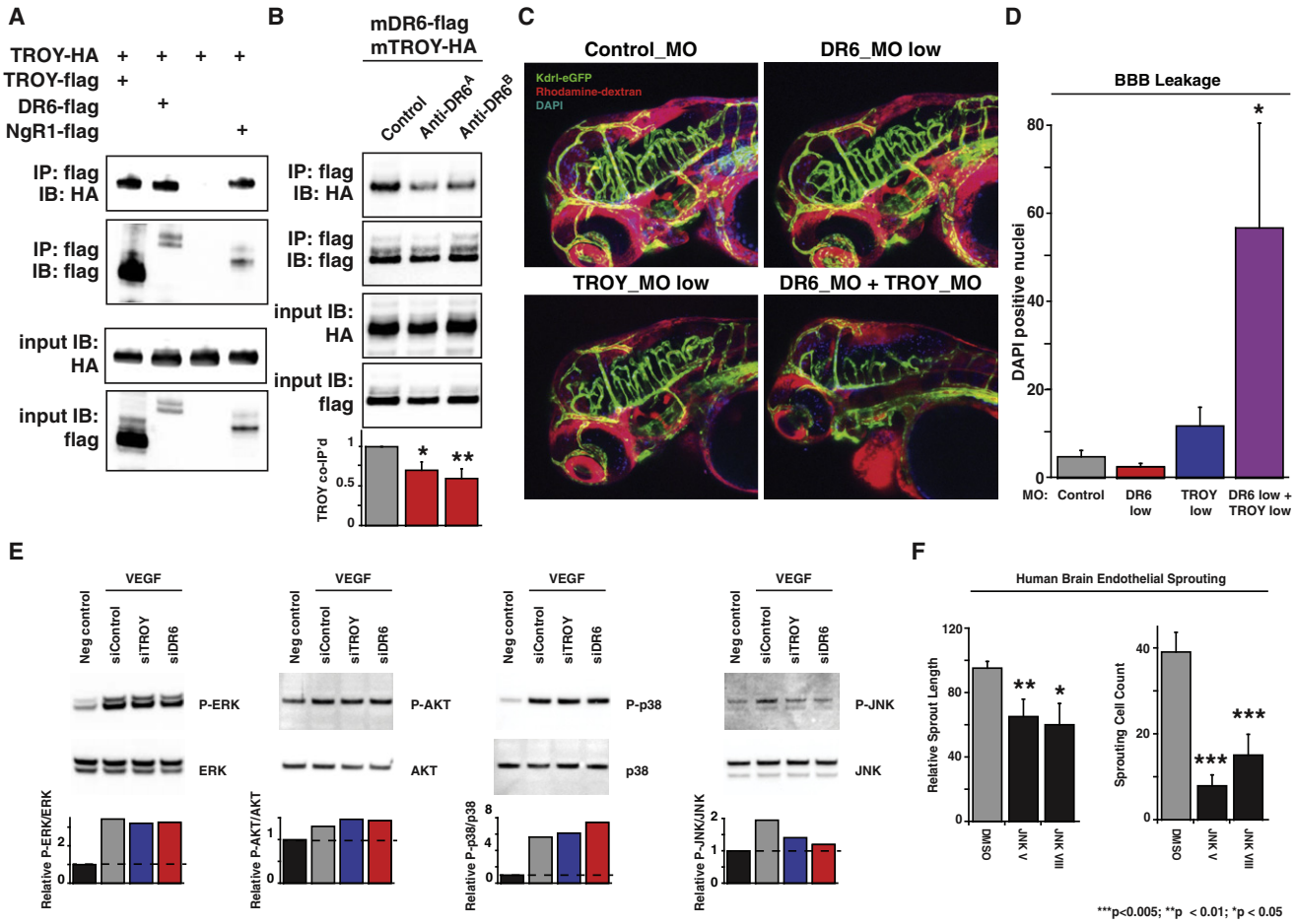

Figure 6. DR6 and TROY Physically and Genetically Interact and Are Required for VEGF-Mediated JNK Activation

(A) DR6 physically interacts with TROY. Epitope-tagged receptors were overexpressed in COS-7 cells and flag-tagged TROY bait was immunoprecipitated. Input was 1% total cellular lysate used in pulldown. IP, immunoprecipitation; IB, immunoblot. Results representative of at least three independent experiments are shown.

(B) Anti-DR6 function-blocking antibodies, which inhibit human brain endothelial sprouting, also reduce DR6 and TROY physical interaction. Pulldown assays were carried out as described above with the addition of anti-DR6 antibodies four hours after transfection. Relative TROY coimmunoprecipitation was calculated by normalization to both TROY-HA input and DR6-flag pulldown levels. Results representative of at least three independent experiments are shown.

(C) Suboptimal concentrations of *DR6*- and *TROY*-targeting morpholinos unmask genetic interactions. Each embryo was treated with 4 ng of each splice-blocking morpholino. Endothelial cells are green, DAPI is blue, rhodamine-dextran is red. Results representative of at least three independent experiments are shown.

(D) Quantification of DAPI leakage reveals *DR6* and *TROY* genetic interaction. n = 8 (control_MO), n = 8 (DR6_MO), n = 8 (TROY_MO), n = 8 (DR6_MO and TROY_MO).

(E) VEGF activates JNK in HBMECs and requires *DR6* and *TROY* expression. Relative protein phosphorylation was calculated by normalization to total protein levels. Results representative of at least three independent experiments are shown.

(F) JNK activity is required for HBMEC sprouting. 1 μM JNK inhibitor V or VIII was used.

Data are presented as the mean ± SEM (***p < 0.005; **p < 0.01; *p < 0.05). See also Figure S6.

Death Receptor Crosstalk with VEGF-VEGFR2 Signaling

In addition to the signaling kinases p38, ERK, and AKT, we find that the VEGF-VEGFR2 pathway activates JNK in human brain endothelial cells in a DR6 and TROY-dependent fashion. We postulate that death receptors directly interface with the downstream signaling elements of the VEGF-VEGFR pathway in order to effectively modulate sprouting angiogenesis. This signaling axis would then allow for the integration of signaling input from both VEGF ligands and death receptors. Consistent with this hypothesis, p75 activity has been shown to promote endothelial cell apoptosis and inhibit angiogenesis through modulating VEGF signaling by inhibition of AKT (Caporali et al., 2008).

Death Receptor Regulation in CNS Vasculature

It remains to be determined if DR6 and TROY function in a ligand-independent fashion, or if DR6 and TROY act as coreceptors for an unidentified ligand to mediate CNS vascular biology. Notably, TNF receptor family members including TNFRSF1A/TNFR, TNFRSF10B/DR5, and TNFRSF5/CD40 can assemble into pre-formed trimer complexes in the absence of cognate ligand

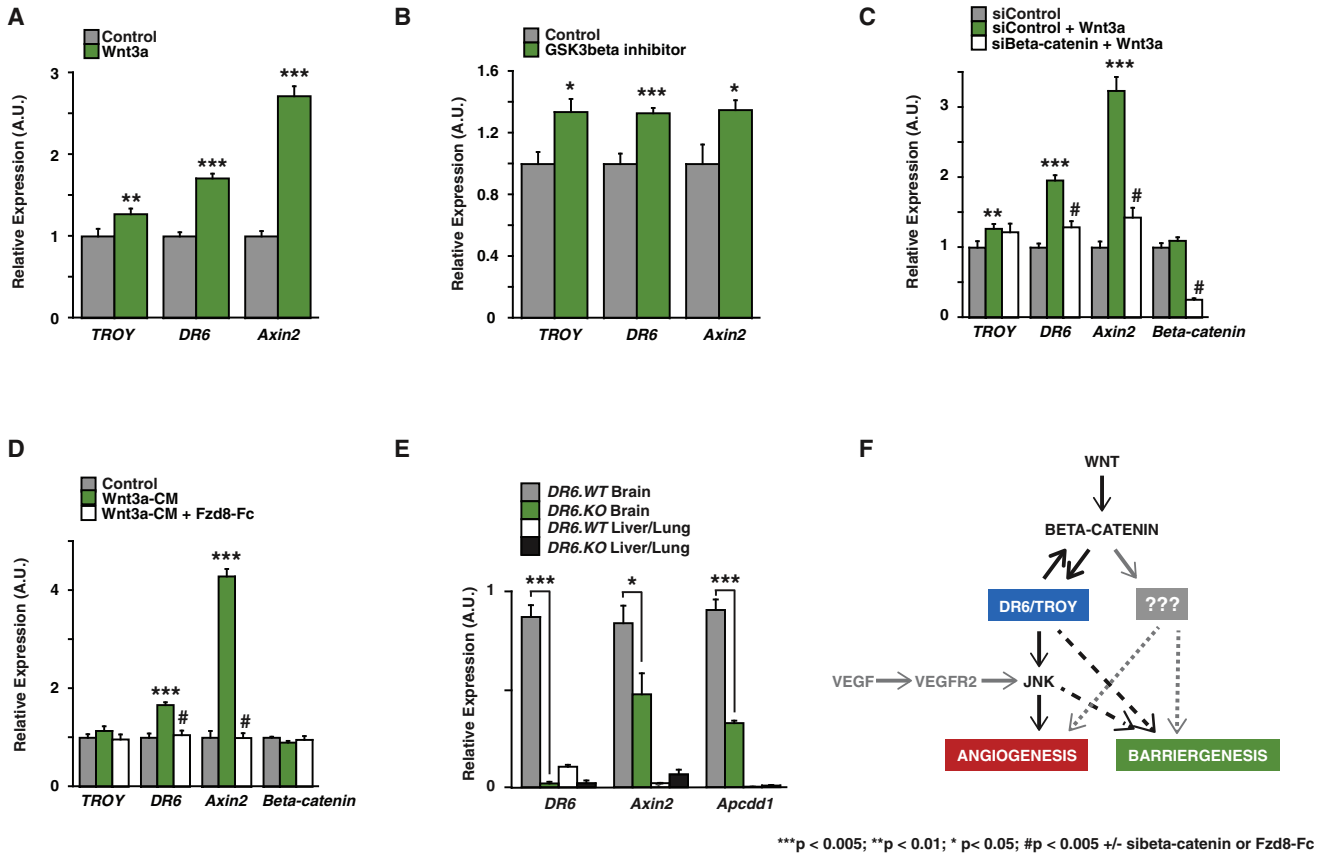

Figure 7. *DR6* and *TROY* Are Downstream of Canonical Wnt/Beta-Catenin Signaling in CNS Vasculature

(A) Wnt3a ligand stimulates *DR6* and *TROY* expression in human brain endothelial cells. Recombinant human Wnt3a (200 ng/ml) was added to HBMECs and RNA was analyzed 24 hr postligand addition by qPCR.

(B) Increased beta-catenin levels stimulate *DR6* and *TROY* expression in human brain endothelial cells. GSK3beta inhibitor SB216763 (20 μM) was added to HBMECs and analyzed as described above.

(C) Recombinant Wnt3a-mediated *DR6* and *TROY* expression is dependent on *beta-catenin*. HBMEC RNA was analyzed as above 24 hr after Wnt3a addition ± siRNA targeting beta-catenin.

(D) Wnt3a-conditioned media stimulates *DR6* and *TROY* expression in a ligand-dependent fashion. HBMEC RNA was analyzed as above 24 hr after Wnt3a-CM addition ± pan-Wnt binding Fzd8-Fc.

(E) Wnt signaling in embryonic mouse brain vasculature is attenuated upon *DR6* knockout. CD31+CD45- vasculature was FACS-purified as in Figure S1A and analyzed as described above.

(F) Model for death receptors DR6 and TROY function in BBB development. Wnt ligands secreted by the embryonic neuroepithelium stabilize beta-catenin protein levels in CNS endothelial cells which subsequently upregulates, among many other target genes, DR6 and TROY expression. DR6, and possibly TROY, participate in a Wnt/beta-catenin positive feedback loop whereby signaling is amplified by these death receptors through an unknown mechanism. Through JNK activation, these receptors engage in crosstalk with the VEGF/VEGFR2 signaling pathway to drive CNS angiogenesis and possibly barriergenesis.

Data are presented as the mean ± SEM (***p < 0.005; **p < 0.01; *p < 0.05; #p < 0.005 comparing Wnt3a ± Fzd8-Fc or sibeta-catenin). See also Figure S7.

binding (Chan et al., 2000), while TNFRSF8/CD30 overexpression has been shown to drive downstream NF-κB signaling in a ligand-independent fashion (Horie et al., 2002). Thus, it is possible that DR6 and TROY function at the BBB as a ligand-independent signaling unit.

Importantly, we found that DR6 and TROY are coregulated at the BBB. In addition to exhibiting similar loss-of-function phenotypes, these two death receptors physically and genetically interact, and have overlapping expression patterns. Recently, both in silico transcription factor binding prediction and expression profiling studies to identify Wnt/beta-catenin target genes in human fibroblasts, dermal papilli, and stromal stem cells found both *DR6* and *TROY* as potential downstream effectors (Hödar et al., 2010; Klapholz-Brown et al., 2007; Qiu et al., 2010; Shin et al., 2010). Accordingly, we find that *DR6* and *TROY* are downstream target genes of canonical Wnt/beta-catenin signaling in human brain endothelium, which is exclusively activated in CNS-specific endothelial cells during development. Considering that loss of Wnt/beta-catenin signaling results in more severe BBB developmental defects when compared to DR6 and TROY loss of function, it must be the case that DR6 and TROY work in concert with other Wnt target genes to fully regulate CNS angiogenesis and barriergenesis. Nevertheless, our results provide a mechanistic explanation of how DR6 and TROY coexpression is regulated at the BBB. Specifically, *DR6* and *TROY* are expressed in CNS endothelial cells through

neuroepithelium-derived Wnt ligands and subsequent induction of Wnt/beta-catenin transcriptional target genes. It is through the expression of these particular death receptors, as well as other unidentified components, that Wnt/beta-catenin signaling regulates organ-specific formation and differentiation of CNS vasculature.

EXPERIMENTAL PROCEDURES

Zebrafish Microangiographic Imaging and Quantification

Microangiography and live imaging of brain vascularization were adapted from (Jeong et al., 2008; Lawson and Weinstein, 2002). For microangiographic assessment of BBB integrity, morpholino-injected embryos were anesthetized at 3.25 dpf in 0.04% tricaine pH 7 (Sigma E10521), and injected with 12 nl of 12.5 mg/ml rhodamine-dextran and 0.85 mg/ml DAPI mix into the common cardinal vein. Embryos were mounted in 1% low-melt agarose in Danieau buffer (58 mM NaCl, 0.7 mM KCl, 0.4 mM $MgSO_4$, 0.6 mM $Ca[NO_3]_2$, and 5 mM HEPES [pH 7.6]) containing tricaine in a glass-bottom 96-well plate, and z stacks (~100 μm thick, 3 μm spacing between sagittal planes, three line averages) were collected within 30 min of injection. All images were acquired using a laser scanning confocal microscope (TCS SP5, Leica) with a 500 mW Argon-Ion laser (LASOS) and a 20× air objective (Apochromat 0.7 NA, Leica).

The integrity of the BBB and extent of brain vascularization were quantified in control and morpholino-injected fish from two dimensional (2D) maximum z projections and three dimensional (3D) renderings of the z stacks. 2D maximum z projections were created using ImageJ (developed by the National Institutes of Health), and the number of DAPI positive brain parenchymal nuclei was manually counted for each condition ($n > 6$ animals per condition). DAPI-positive brain parenchymal nuclei were visually isolated using Adobe Photoshop CS5 subtraction blending whereby DAPI+GFP+ double-positive signal (DAPI labeling of brain vasculature) was computationally removed from the DAPI channel. 2D z projections were also used to quantify the fractional height of the central arteries (CtA) penetrating into the embryo brain by normalizing CtA height against the height of the dorsal longitudinal vein (DLV) above the junction of the posterior communicating segment (PCS) and the basilar artery (BA). Similarly, the fractional height of ISVs was calculated relative to the separation of the dorsal aorta from the dorsal longitudinal anastomotic vessel.

The brain vasculature was reconstructed in 3D by first deconvolving the z stacks using AutoQuant X (AutoQuant Imaging) and then 3D rendering with Imaris (Bitplane). Quantification of total length and volume of CtAs in the left hindbrain, and number of branches within this network of CtAs were performed using the Surface Tool and Filament Tracking packages in Imaris. Both surface rendering and filament tracking were conducted using default parameters whenever possible; however, manual correction of the filament tracking results, using the raw fluorescence signal as a guide, was often necessary. Vessel and branch density were subsequently calculated by normalizing against the volume of the left hindbrain. Brain volume was approximated as $V = R_1R_2R_3$, where R_1 is the length of the BA, R_2 is the height of the DLV above the junction of the PCS and BA, and R_3 is the distance from to the primordial hindbrain channel (PHBC) to the junction of the PCS and BA, measured perpendicular to the BA (Figure 3E).

Live imaging of vascularization in the zebrafish brain was carried out as above with a few modifications: 5–20 embryos were dechorionated at 1–3 dpf and embedded in 1% low-melt agarose in Danieau buffer containing tricaine and 0.03 mg/ml N-phenylthiourea (PTU; Sigma P7629) at 28.5°C. The coordinates of each embryo were stored using a motorized stage (Märzhäuser Wetzlar) and time-lapse images were acquired every 10–30 min for up to 12 hr. The embryo stage and frame rate and total duration of imaging are provided with the supplemental movies.

Primary Human Brain Microvascular Endothelial Cell Culture and Bead Outgrowth Assay

HBMECs from Cell Systems (ACBRI 376) were maintained in Lonza EGM2 SingleQuots (CC-3162). Dharmacon ON-TARGET*plus* SMARTpool siRNAs were transfected in primary cells using Dharmafect transfection reagent #1 (T-2001) according to the manufacturer's instructions. Small molecule inhibitors, including JNK inhibitor V (Calbiochem AS601245), JNK VIII inhibitor (Calbiochem 420135), and GSK3beta inhibitor SB216763 (Tocris 1616), were added 24 hr before cell lysis. The bead outgrowth assay was adapted from (Nakatsu et al., 2003). In brief, hydrated collagen-coated dextran beads (Amersham Cytodex-3 17-0485-01) were coated with HBMECs (300 cells/bead) by shaking cells every 10–30 min for 3 hr and allowed to grow in a flask overnight in 10 ml fresh media. Fibrinogen (25 mg/ml; Sigma F8630) was made in EGM2 and diluted 10-fold in bead medium. Bead medium consists of EGM2, 1:5 human skin fibroblast-conditioned media (ATCC CCL-110 in EGM2), 2 ng/ml hVEGF, and 2 ng/ml HGF. Two hundred HBMEC-coated beads/ml released from the flask bottom by aggressive tapping were washed and added into fibrinogen/bead medium mixture and 1 ml pipetted into wells of 12 well plate with 10 μl thrombin (Sigma T9549). After 20 min in 37°C incubator, 2 ml bead media was slowly added to the fibrin gel matrix along with function-blocking antibodies or small molecule inhibitors. Cells were fixed 1% PFA in PBS overnight at 4°C, washed twice in PBS, and stained in PBS with 1:10,000 Hoescht and 1:250 Phalloidin-488 conjugate (Invitrogen A12379) overnight at 4°C. After two PBS washes, confocal z stacks of the entire plate was acquired using the ImageXpress Micro (Molecular Devices). Mean sprout lengths were calculated by manual tracing and the number of sprouting cells were counted automatically using ImageJ.

Animals

Mice, zebrafish, and their embryos were handled in accordance with Genentech IACUC guidelines.

SUPPLEMENTAL INFORMATION

Supplemental Information includes seven figures, Supplemental Experimental Procedures, one table, and six movies and can be found with this article online at doi:10.1016/j.devcel.2011.11.018.

ACKNOWLEDGMENTS

We thank members of the Watts laboratory, Anatoly Nikolaev, Sidney Hsieh, Joe Lewcock, Kyle Niessen, Bob Liu, David Simon, Jeremy Burton, Philip Vitorino, James Ernst, and John Brady Ridgway for kindly providing reagents, advice, and stimulating discussions. We thank Murat Yaylaoglu for in situ hybridization experiments, Rupak Neupane, Laurie L. Gilmour, Chungkee Poon, and James E. Cupp for FACS sorting and analysis, Jed Ross for ex vivo mouse brain imaging techniques, Cecile Chalouni and Laszlo Komuves for confocal microscopy guidance, and Janice Maloney for subcloning *TROY* expression constructs. All authors are paid employees of Genentech.

Received: June 8, 2011
Revised: October 7, 2011
Accepted: November 14, 2011
Published online: February 13, 2012

REFERENCES

Adams, R.H., and Alitalo, K. (2007). Molecular regulation of angiogenesis and lymphangiogenesis. Nat. Rev. Mol. Cell Biol. *8*, 464–478.

Ashkenazi, A., and Dixit, V.M. (1998). Death receptors: signaling and modulation. Science *281*, 1305–1308.

Beg, A.A., and Baltimore, D. (1996). An essential role for NF-kappaB in preventing TNF-alpha-induced cell death. Science *274*, 782–784.

Caporali, A., Pani, E., Horrevoets, A.J., Kraenkel, N., Oikawa, A., Sala-Newby, G.B., Meloni, M., Cristofaro, B., Graiani, G., Leroyer, A.S., et al. (2008). Neurotrophin p75 receptor (p75NTR) promotes endothelial cell apoptosis and inhibits angiogenesis: implications for diabetes-induced impaired neovascularization in ischemic limb muscles. Circ. Res. *103*, e15–e26.

Chan, F.K., Chun, H.J., Zheng, L., Siegel, R.M., Bui, K.L., and Lenardo, M.J. (2000). A domain in TNF receptors that mediates ligand-independent receptor assembly and signaling. Science *288*, 2351–2354.

Chen, J., Somanath, P.R., Razorenova, O., Chen, W.S., Hay, N., Bornstein, P., and Byzova, T.V. (2005). Akt1 regulates pathological angiogenesis, vascular maturation and permeability in vivo. Nat. Med. *11*, 1188–1196.

Chen, L., Park, S.M., Tumanov, A.V., Hau, A., Sawada, K., Feig, C., Turner, J.R., Fu, Y.X., Romero, I.L., Lengyel, E., and Peter, M.E. (2010). CD95 promotes tumour growth. Nature *465*, 492–496.

Daneman, R., Agalliu, D., Zhou, L., Kuhnert, F., Kuo, C.J., and Barres, B.A. (2009). Wnt/beta-catenin signaling is required for CNS, but not non-CNS, angiogenesis. Proc. Natl. Acad. Sci. USA *106*, 641–646.

Daneman, R., Zhou, L., Agalliu, D., Cahoy, J.D., Kaushal, A., and Barres, B.A. (2010). The mouse blood-brain barrier transcriptome: a new resource for understanding the development and function of brain endothelial cells. PLoS ONE *5*, e13741.

DeAlmeida, V.I., Miao, L., Ernst, J.A., Koeppen, H., Polakis, P., and Rubinfeld, B. (2007). The soluble wnt receptor Frizzled8CRD-hFc inhibits the growth of teratocarcinomas in vivo. Cancer Res. *67*, 5371–5379.

Eby, M.T., Jasmin, A., Kumar, A., Sharma, K., and Chaudhary, P.M. (2000). TAJ, a novel member of the tumor necrosis factor receptor family, activates the c-Jun N-terminal kinase pathway and mediates caspase-independent cell death. J. Biol. Chem. *275*, 15336–15342.

Ek, C.J., Dziegielewska, K.M., Stolp, H., and Saunders, N.R. (2006). Functional effectiveness of the blood-brain barrier to small water-soluble molecules in developing and adult opossum (Monodelphis domestica). J. Comp. Neurol. *496*, 13–26.

Eliceiri, B.P., Paul, R., Schwartzberg, P.L., Hood, J.D., Leng, J., and Cheresh, D.A. (1999). Selective requirement for Src kinases during VEGF-induced angiogenesis and vascular permeability. Mol. Cell *4*, 915–924.

Gaillard, P., Jeanclaude-Etter, I., Ardissone, V., Arkinstall, S., Cambet, Y., Camps, M., Chabert, C., Church, D., Cirillo, R., Gretener, D., et al. (2005). Design and synthesis of the first generation of novel potent, selective, and in vivo active (benzothiazol-2-yl)acetonitrile inhibitors of the c-Jun N-terminal kinase. J. Med. Chem. *48*, 4596–4607.

Gerber, H.P., Dixit, V., and Ferrara, N. (1998). Vascular endothelial growth factor induces expression of the antiapoptotic proteins Bcl-2 and A1 in vascular endothelial cells. J. Biol. Chem. *273*, 13313–13316.

Gong, Y., Bourhis, E., Chiu, C., Stawicki, S., DeAlmeida, V.I., Liu, B.Y., Phamluong, K., Cao, T.C., Carano, R.A., Ernst, J.A., et al. (2010). Wnt isoform-specific interactions with coreceptor specify inhibition or potentiation of signaling by LRP6 antibodies. PLoS ONE *5*, e12682.

Gu, C., Rodriguez, E.R., Reimert, D.V., Shu, T., Fritzsch, B., Richards, L.J., Kolodkin, A.L., and Ginty, D.D. (2003). Neuropilin-1 conveys semaphorin and VEGF signaling during neural and cardiovascular development. Dev. Cell *5*, 45–57.

Hallmann, R., Mayer, D.N., Berg, E.L., Broermann, R., and Butcher, E.C. (1995). Novel mouse endothelial cell surface marker is suppressed during differentiation of the blood brain barrier. Dev. Dyn. *202*, 325–332.

Hödar, C., Assar, R., Colombres, M., Aravena, A., Pavez, L., González, M., Martínez, S., Inestrosa, N.C., and Maass, A. (2010). Genome-wide identification of new Wnt/beta-catenin target genes in the human genome using CART method. BMC Genomics *11*, 348.

Horie, R., Watanabe, T., Morishita, Y., Ito, K., Ishida, T., Kanegae, Y., Saito, I., Higashihara, M., Mori, S., Kadin, M.E., and Watanabe, T. (2002). Ligand-independent signaling by overexpressed CD30 drives NF-kappaB activation in Hodgkin-Reed-Sternberg cells. Oncogene *21*, 2493–2503.

Jeong, J.Y., Kwon, H.B., Ahn, J.C., Kang, D., Kwon, S.H., Park, J.A., and Kim, K.W. (2008). Functional and developmental analysis of the blood-brain barrier in zebrafish. Brain Res. Bull. *75*, 619–628.

Jin, S.W., Beis, D., Mitchell, T., Chen, J.N., and Stainier, D.Y. (2005). Cellular and molecular analyses of vascular tube and lumen formation in zebrafish. Development *132*, 5199–5209.

Klapholz-Brown, Z., Walmsley, G.G., Nusse, Y.M., Nusse, R., and Brown, P.O. (2007). Transcriptional program induced by Wnt protein in human fibroblasts suggests mechanisms for cell cooperativity in defining tissue microenvironments. PLoS ONE *2*, e945.

Laukeviciene, A., Brecht, S., Kevelaitis, E., and Herdegen, T. (2006). Enhanced contractility of small blood vessels in JNK knockout mice. Eur. J. Pharm. Sci. *29*, 335–339.

Lavrik, I.N., Golks, A., Riess, D., Bentele, M., Eils, R., and Krammer, P.H. (2007). Analysis of CD95 threshold signaling: triggering of CD95 (FAS/APO-1) at low concentrations primarily results in survival signaling. J. Biol. Chem. *282*, 13664–13671.

Lawson, N.D., and Weinstein, B.M. (2002). In vivo imaging of embryonic vascular development using transgenic zebrafish. Dev. Biol. *248*, 307–318.

Liebner, S., Corada, M., Bangsow, T., Babbage, J., Taddei, A., Czupalla, C.J., Reis, M., Felici, A., Wolburg, H., Fruttiger, M., et al. (2008). Wnt/beta-catenin signaling controls development of the blood-brain barrier. J. Cell Biol. *183*, 409–417.

Logan, C.Y., and Nusse, R. (2004). The Wnt signaling pathway in development and disease. Annu. Rev. Cell Dev. Biol. *20*, 781–810.

Nakatsu, M.N., Sainson, R.C., Aoto, J.N., Taylor, K.L., Aitkenhead, M., Pérez-del-Pulgar, S., Carpenter, P.M., and Hughes, C.C. (2003). Angiogenic sprouting and capillary lumen formation modeled by human umbilical vein endothelial cells (HUVEC) in fibrin gels: the role of fibroblasts and Angiopoietin-1. Microvasc. Res. *66*, 102–112.

Nikolaev, A., McLaughlin, T., O'Leary, D.D., and Tessier-Lavigne, M. (2009). APP binds DR6 to trigger axon pruning and neuron death via distinct caspases. Nature *457*, 981–989.

Pan, G., Bauer, J.H., Haridas, V., Wang, S., Liu, D., Yu, G., Vincenz, C., Aggarwal, B.B., Ni, J., and Dixit, V.M. (1998). Identification and functional characterization of DR6, a novel death domain-containing TNF receptor. FEBS Lett. *431*, 351–356.

Pan, Q., Chanthery, Y., Liang, W.C., Stawicki, S., Mak, J., Rathore, N., Tong, R.K., Kowalski, J., Yee, S.F., Pacheco, G., et al. (2007). Blocking neuropilin-1 function has an additive effect with anti-VEGF to inhibit tumor growth. Cancer Cell *11*, 53–67.

Pardridge, W.M., Boado, R.J., and Farrell, C.R. (1990). Brain-type glucose transporter (GLUT-1) is selectively localized to the blood-brain barrier. Studies with quantitative western blotting and in situ hybridization. J. Biol. Chem. *265*, 18035–18040.

Park, J.B., Yiu, G., Kaneko, S., Wang, J., Chang, J., He, X.L., Garcia, K.C., and He, Z. (2005). A TNF receptor family member, TROY, is a coreceptor with Nogo receptor in mediating the inhibitory activity of myelin inhibitors. Neuron *45*, 345–351.

Pedram, A., Razandi, M., and Levin, E.R. (1998). Extracellular signal-regulated protein kinase/Jun kinase cross-talk underlies vascular endothelial cell growth factor-induced endothelial cell proliferation. J. Biol. Chem. *273*, 26722–26728.

Qiu, W., Hu, Y., Andersen, T.E., Jafari, A., Li, N., Chen, W., and Kassem, M. (2010). Tumor necrosis factor receptor superfamily member 19 (TNFRSF19) regulates differentiation fate of human mesenchymal (stromal) stem cells through canonical Wnt signaling and C/EBP. J. Biol. Chem. *285*, 14438–14449.

Rousseau, S., Houle, F., Landry, J., and Huot, J. (1997). p38 MAP kinase activation by vascular endothelial growth factor mediates actin reorganization and cell migration in human endothelial cells. Oncogene *15*, 2169–2177.

Rubin, L.L., and Staddon, J.M. (1999). The cell biology of the blood-brain barrier. Annu. Rev. Neurosci. *22*, 11–28.

Schnepp, A., Komp Lindgren, P., Hülsmann, H., Kröger, S., Paulsson, M., and Hartmann, U. (2005). Mouse testican-2. Expression, glycosylation, and effects on neurite outgrowth. J. Biol. Chem. *280*, 11274–11280.

Shao, Z., Browning, J.L., Lee, X., Scott, M.L., Shulga-Morskaya, S., Allaire, N., Thill, G., Levesque, M., Sah, D., McCoy, J.M., et al. (2005). TAJ/TROY, an orphan TNF receptor family member, binds Nogo-66 receptor 1 and regulates axonal regeneration. Neuron *45*, 353–359.

Shin, H., Kwack, M.H., Shin, S.H., Oh, J.W., Kang, B.M., Kim, A.A., Kim, J., Kim, M.K., Kim, J.C., and Sung, Y.K. (2010). Identification of transcriptional targets of Wnt/beta-catenin signaling in dermal papilla cells of human scalp hair follicles: EP2 is a novel transcriptional target of Wnt3a. J. Dermatol. Sci. *58*, 91–96.

Six, I., Kureishi, Y., Luo, Z., and Walsh, K. (2002). Akt signaling mediates VEGF/VPF vascular permeability in vivo. FEBS Lett. *532*, 67–69.

Stenman, J.M., Rajagopal, J., Carroll, T.J., Ishibashi, M., McMahon, J., and McMahon, A.P. (2008). Canonical Wnt signaling regulates organ-specific assembly and differentiation of CNS vasculature. Science *322*, 1247–1250.

Szczepankiewicz, B.G., Kosogof, C., Nelson, L.T., Liu, G., Liu, B., Zhao, H., Serby, M.D., Xin, Z., Liu, M., Gum, R.J., et al. (2006). Aminopyridine-based c-Jun N-terminal kinase inhibitors with cellular activity and minimal cross-kinase activity. J. Med. Chem. *49*, 3563–3580.

Takahashi, T., Ueno, H., and Shibuya, M. (1999). VEGF activates protein kinase C-dependent, but Ras-independent Raf-MEK-MAP kinase pathway for DNA synthesis in primary endothelial cells. Oncogene *18*, 2221–2230.

Tam, S.J., and Watts, R.J. (2010). Connecting vascular and nervous system development: angiogenesis and the blood-brain barrier. Annu. Rev. Neurosci. *33*, 379–408.

Tong, A.H., Evangelista, M., Parsons, A.B., Xu, H., Bader, G.D., Pagé, N., Robinson, M., Raghibizadeh, S., Hogue, C.W., Bussey, H., et al. (2001). Systematic genetic analysis with ordered arrays of yeast deletion mutants. Science *294*, 2364–2368.

Uchida, C., Gee, E., Ispanovic, E., and Haas, T.L. (2008). JNK as a positive regulator of angiogenic potential in endothelial cells. Cell Biol. Int. *32*, 769–776.

Vasudevan, A., Long, J.E., Crandall, J.E., Rubenstein, J.L., and Bhide, P.G. (2008). Compartment-specific transcription factors orchestrate angiogenesis gradients in the embryonic brain. Nat. Neurosci. *11*, 429–439.

Virgintino, D., Girolamo, F., Errede, M., Capobianco, C., Robertson, D., Stallcup, W.B., Perris, R., and Roncali, L. (2007). An intimate interplay between precocious, migrating pericytes and endothelial cells governs human fetal brain angiogenesis. Angiogenesis *10*, 35–45.

Wang, K.C., Kim, J.A., Sivasankaran, R., Segal, R., and He, Z. (2002). P75 interacts with the Nogo receptor as a co-receptor for Nogo, MAG and OMgp. Nature *420*, 74–78.

Wu, G., Luo, J., Rana, J.S., Laham, R., Sellke, F.W., and Li, J. (2006). Involvement of COX-2 in VEGF-induced angiogenesis via P38 and JNK pathways in vascular endothelial cells. Cardiovasc. Res. *69*, 512–519.